FOREX Publication
Open Access | Rapid and quality publishing

International Journal of
Electrical and Electronics Research (IJEER)
Research Article | Volume 14, Issue 1| Pages 64-72|e-ISSN: 2347-470X

A Simplified Continuous PWM Using Nearest Four Vectors Based on 2L-SVM for Common-Mode Voltage Reduction in Vienna T-Type Rectifier

Kanyarat Ek-iam[1], and Ong-ard Tubburee[2*]

[1]Department of Industrial Electrical Technology, Faculty of Industrial Technology, Valaya Alongkorn Rajabhat University under the Royal Patronage, Pathum Thani, Thailand; kanyarat@vru.ac.th
[2]Department of Industrial Electrical Technology, Faculty of Industrial Technology, Valaya Alongkorn Rajabhat University under the Royal Patronage, Pathum Thani, Thailand; ongart.tub@vru.ac.th

***Correspondence:** *Ong-ard Tubburee; ongart.tub@vru.ac.th; Tel.: +668-6618-0069*

ABSTRACT- Vienna rectifiers are widely employed in high-performance DC power conversion systems, including electric vehicle (EV) charging infrastructure, renewable energy systems, telecommunication infrastructure, and uninterruptible power supplies (UPS). This paper presents a simplified continuous pulse-width modulation (PWM) strategy for the Vienna T-type rectifier, developed using the nearest four vectors derived from the two-level space vector modulation (2L-SVM) principle. The proposed method restructures the switching-state sequence across twelve updated sectors and incorporates a unified zero-sequence injection scheme to satisfy the inherent operating constraint (OC) while ensuring fully continuous modulation. The resulting symmetric seven-segment switching sequence improves voltage synthesis, keeps the neutral-point (NP) voltage balance, and greatly reduces common-mode voltage (CMV). Simulation results obtained from MATLAB/Simulink confirm that the proposed method generates smoother line-to-line voltage waveforms, reduces the CMV RMS level by 19.71% compared with the conventional discontinuous SVPWM, and achieves high-quality sinusoidal input currents with a THD of 2.49%, well within the IEEE 519 limit. These results indicate that the proposed modulation strategy is an effective, simple, and hardware-independent way to convert AC to DC with high efficiency in modern power electronics.

Keywords: Vienna T-type rectifier, Nearest four vectors, Common-mode voltage, Zero-sequence component.

ARTICLE INFORMATION

Author(s): Kanyarat Ek-iam, and Ong-ard Tubburee;
Received: 26/11/2025; **Accepted**: 29/01/2026; **Published**: 10/03/2026;
E- ISSN: 2347-470X;
Paper Id: IJEER2611A17
Citation: 10.37391/ijeer.140107
Webpage-link:
https://ijeer.forexjournal.co.in/archive/volume-14/ijeer-140107.html

Publisher's Note: FOREX Publication stays neutral with regard to jurisdictional claims in Published maps and institutional affiliations.

1. INTRODUCTION

The demand for high-efficiency AC–DC power conversion has grown rapidly in various applications, such as electric vehicle (EV) fast charging, renewable energy systems, telecommunication infrastructure, and uninterruptible power supplies (UPS) [1,2]. To address this demand, various three-phase rectifier technologies have been developed and can be generally classified into three categories: passive, hybrid, and active rectifiers [3-5]. Among them, active rectifiers have attracted particular interest due to their ability to meet stringent power quality (PQ) standards such as IEEE 519 and IEC 61000-3, offering near-unity power factor (PF) and low current harmonic distortion. The Vienna rectifiers have emerged as one of the most promising unidirectional AC–DC converter topologies, combining high efficiency and lower semiconductor voltage stress—limited to half of the DC-link voltage. These characteristics result in improved power density, reliability, and overall system performance, making it suitable for compact and high-performance power conversion systems. Structurally, Vienna rectifiers can be implemented in three main configurations: the 3-switch, 6-switch, and T-type topologies. Among these, the Vienna T-type rectifier (*figure 1*) has attracted the most attention due to its optimal balance between circuit complexity and performance. With conversion efficiencies ranging from 94% to 99% [6], it has proven highly effective in achieving low losses and superior power quality. Based on rectification principles, the primary objective of a rectifier is to transfer the input current with the highest instantaneous magnitude to the load while satisfying the operating constraint (OC)—the polarity of each phase voltage must match that of its current [7]. In the Vienna T-type rectifier, the presence of input filter inductors on the AC side introduces a phase shift between voltage and current, violating this OC and causing input-current distortion. Various control and modulation strategies have been proposed to mitigate this effect and improve PF. Early methods, such as hysteresis current control [8], achieved sinusoidal input currents without explicit modulation but suffered from variable switching frequency. Carrier-based PWM (CB-PWM) methods [9], ensured constant switching frequency and digital simplicity but exhibited limited DC-link utilization and required complex zero-sequence injection for neutral-point (NP) balancing. Alternatively, space-vector modulation (SVM) has been widely

FOREX Publication
Open Access | Rapid and quality publishing
International Journal of Electrical and Electronics Research (IJEER)
Research Article | Volume 14, Issue 1| Pages 64-72|e-ISSN: 2347-470X

adopted in Vienna rectifiers owing to its superior current quality, NP-voltage balancing, and reduced total harmonic distortion (THD) [10]. However, its implementation is computationally complex, and the three switching states corresponding to each voltage vector in a space-vector diagram cannot be directly utilized, as they violate the OC. To address these issues, the space-vector PWM (SVPWM) techniques have been proposed, combining the advantages of CB-PWM and conventional SVM. The discontinuous SVPWM method in [11,12] clamps one phase leg during the highest instantaneous current interval, improving NP-voltage balance and lowering THD. However, this discontinuous switching behavior generates high common-mode voltage (CMV), increasing leakage current, electromagnetic interference (EMI), and potential system instability [13].

Although hardware-based CMV suppression techniques using active or passive filters have been explored [14], they introduce additional cost and efficiency loss. Consequently, modulation-based CMV reduction has become a preferred research direction. Continuous PWM strategies proposed in [7] and [15] reduced CMV by rearranging switching sequences and injecting zero-sequence components based on current polarity. However, when the control signals are generated based on the three-level space vector modulation (3L-SVM) framework, operation at high modulation indices tends to induce DC-link capacitor voltage imbalance due to the absence of effective zero-vector utilization, thereby requiring auxiliary control loops for stabilization. To overcome these limitations, this paper proposes a simplified continuous PWM strategy based on the nearest four voltage vectors, comprising two zero vectors and two active vectors, derived from the two-level space vector modulation (2L-SVM) principle, incorporating zero-sequence component injection. The proposed method significantly simplifies implementation by generating gate signals using only eight voltage vectors based on 2L-SVM, whereas 3L-SVM-based approaches typically involve up to twenty-five vectors. Moreover, the proposed strategy inherently maintains DC-link capacitor voltage balance, thereby eliminating the need for auxiliary hardware or additional balancing controllers, while keeping the input current distortion within international harmonic limits. The proposed approach satisfies the OC, reduces CMV, and improves PQ under a conventional voltage-oriented control (VOC) framework [16]. Compared with conventional discontinuous SVPWM, the proposed method achieves effective NP-voltage balancing and reduces current distortion within international harmonic limits. Furthermore, the reduced CMV contributes to lower EMI and leakage current, thereby enhancing overall system reliability and efficiency.

2. TOPOLOGY AND OPERATING PRINCIPLE OF THE VIENNA T-TYPE RECTIFIER

The circuit topology of the Vienna T-type rectifier is illustrated in *figure 1*. The three-phase grid voltages are denoted as e_a, e_b, and e_c, while the corresponding input voltages of the rectifier are v_a, v_b, and v_c, and the input currents are represented by i_a, i_b, and i_c. The DC-link voltage (v_{dc}) consists of two split capacitor voltages, v_{C1} and v_{C2}, corresponding to the upper and lower DC-link capacitors, respectively. On the AC side, three filter inductors, L_a, L_b, and L_c, with equivalent series resistances R_a, R_b, and R_c, are employed to suppress current ripple and improve input power quality. Each phase leg of the rectifier includes two controllable power switches (CPSs)—S_{a1}, S_{a2}, S_{b1}, S_{b2}, and S_{c1}, S_{c2}—connected in series, along with anti-parallel diodes D_{a1}-D_{c2} that allow bidirectional current flow. Fast-recovery diodes D_{aP}–D_{cP} and D_{aN}–D_{cN} are included to handle reverse recovery and minimize switching losses during commutation. The DC-link stage consists of capacitors C_1 and C_2 and a resistive load R_L, with the midpoint between the capacitors forming the NP, denoted as node O.

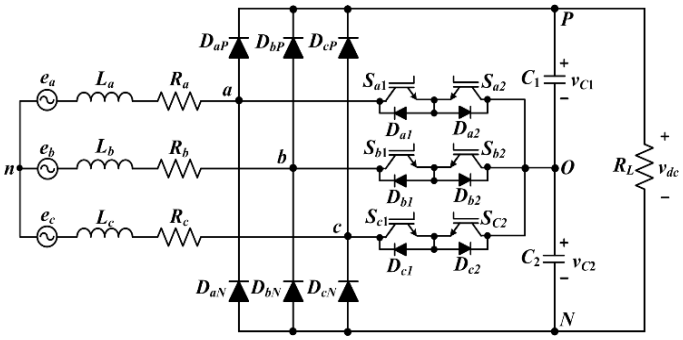

Figure 1. Circuit of the Vienna T-type rectifier

The operation of the proposed rectifier depends on both the direction of the input current and the switching states of the CPSs. Taking the a-phase as an example:

- *Case 1*: Both switches ON — When S_{a1} and S_{a2} are turned ON, point a is connected to the midpoint O. During both positive and negative half-cycles, the current flows through $e_a \rightarrow L_a \rightarrow R_a \rightarrow v_a \rightarrow S_{a1} \rightarrow D_{a2} \rightarrow v_O$, resulting in $v_{aO} = 0$.
- *Case 2*: Both switches OFF (positive current)— When S_{a1} and S_{a2} are turned OFF while $i_a > 0$, point a is connected to the positive DC terminal P. The current flows through $e_a \rightarrow L_a \rightarrow R_a \rightarrow v_a \rightarrow D_{ap} \rightarrow C_1 \rightarrow v_O$, yielding $v_{aO} = +V_{dc}/2$.
- *Case 3*: Both switches OFF (negative current)— When S_{a1} and S_{a2} are turned OFF while $i_a < 0$, point a is connected to the negative DC terminal N. The current flows through $v_O \rightarrow C_2 \rightarrow D_{an} \rightarrow v_a \rightarrow R_a \rightarrow L_a \rightarrow e_a$, resulting in $v_{aO} = -V_{dc}/2$.

From these operating modes, each phase leg of the Vienna T-type topology can generate three voltage levels: $+V_{dc}/2$, 0, and $-V_{dc}/2$. The instantaneous output voltage depends on the combination of switch states and the input current polarity. According to Kirchhoff's Voltage Law (KVL), the instantaneous voltage equation of the a-phase can be expressed as

$$e_a + L\frac{di_a}{dt} + R_a i_a + v_a = v_{nO} \quad (1)$$

FOREX Publication
Open Access | Rapid and quality publishing
International Journal of Electrical and Electronics Research (IJEER)
Research Article | Volume 14, Issue 1| Pages 64-72|e-ISSN: 2347-470X

3. COMMON-MODE VOLTAGE ANALYSIS OF THE VIENNA T-TYPE RECTIFIER

The CMV (v_{On}) of the Vienna T-type rectifier is defined as the potential difference between the midpoint of the split DC-link capacitors (point O) and the neutral point of the AC source (point n) and can be expressed as

$$v_{On} = -\frac{1}{3}(v_{aO} + v_{bO} + v_{cO}) \quad (2)$$

where v_{aO}, v_{bO}, and v_{cO} denote the pole voltages of phases a, b, and c with respect to the DC-link midpoint. Each phase can assume one of three voltage levels—$+V_{dc}/2$, 0, or $-V_{dc}/2$—depending on the instantaneous direction of the input current and the switching states of the bridge arms. The RMS value of the CMV can be calculated using the fundamental AC waveform relation:

$$V_{On,rms} = \sqrt{\frac{1}{T_s}\int_0^{T_s} (v_{On})^2\, dt} \quad (3)$$

where T_s denotes the switching period. Thus, the RMS level of CMV is directly determined by the time-weighted squared magnitude of v_{On}. In the conventional discontinuous PWM strategy, one bridge arm is clamped when its corresponding phase current reaches the highest instantaneous magnitude. Considering the a-phase as an example, when the CPSs of the a-phase bridge arm are clamped and those of the b- and c-phases are actively switching, the CMV exhibits three discrete levels: $V_{dc}/3$, $V_{dc}/6$, and 0, as shown in *figure 2*. Under these conditions, the RMS value of the CMV is approximately 21.52% of the DC-link voltage.

The high RMS level is primarily attributed to the extended duration of the $V_{dc}/3$ segment at the center of the waveform. If the a-phase CPS is allowed to actively switch during this interval, the corresponding pole voltage $+V_{dc}/2$ can partially cancel the CMV, reducing its instantaneous magnitude to $-V_{dc}/6$. However, enabling switching under this condition violates the OC of the rectifier. Therefore, an optimized modulation strategy must be designed to achieve partial CMV cancellation while maintaining input current distortion within acceptable limits specified by the relevant standards.

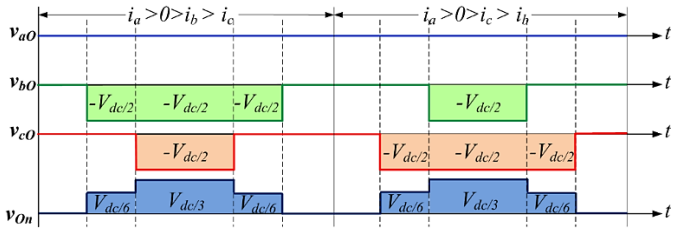

Figure 2. Pole and CMV waveforms obtained using the conventional discontinuous SVPWM when the a-phase current is at its highest positive value

4. METHODOLOGY

4.1. Continuous Command Signals Analysis using the Nearest Four Vectors

The fundamental principle of the SVPWM for a two-level converter is to synthesize a rotating reference voltage vector ($\vec{V}_{ref}$) within a space vector diagram. This vector is synthesized by combining two zero vectors ($\vec{V}_0$ and $\vec{V}_7$) and six active vectors ($\vec{V}_1$–$\vec{V}_6$), as illustrated in *figure 3(a)*. Each vector corresponds to a specific combination of three logic states, known as switching states, which determine the ON/OFF status of the CPSs in each converter leg. The six active vectors are at the corners of the hexagon, and the zero vectors are in the middle. This switching states pattern enables the generation of balanced three-phase voltages that can be continuously modulated according to the desired reference. However, the direct application of conventional SVM switching-state patterns to control the CPSs of the Vienna T-type rectifier is constrained by its OC. Within each 60° sector of the space vector diagram, the phase exhibiting the highest instantaneous input current changes every 30°, altering the valid switching states that comply with the rectifier's current direction.

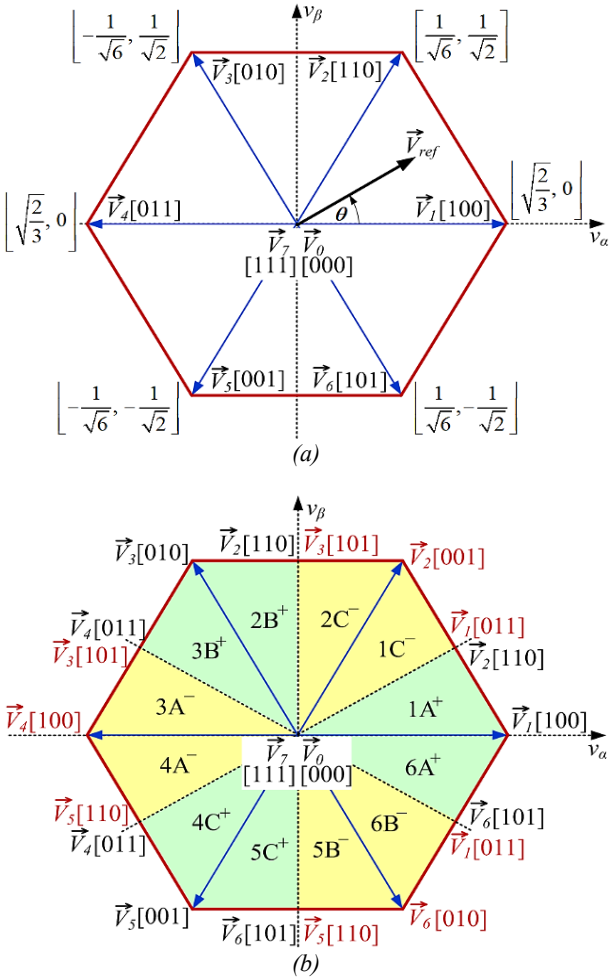

Figure 3. Space vector diagram. (a) Conventional switching state and active vector magnitude, (b) Proposed switching state for a Vienna T-type rectifier

FOREX Publication
Open Access | Rapid and quality publishing
International Journal of Electrical and Electronics Research (IJEER)
Research Article | Volume 14, Issue 1| Pages 64-72|e-ISSN: 2347-470X

For example, in the first conventional sector (0°–60°), the input current flows in the positive direction when the a-phase current is dominant ($i_a>0>i_c>i_b$) and in the negative direction when the c-phase current leads ($i_a>i_b>0>i_c$). Consequently, the entire modulation period is divided into twelve distinct sub-sectors according to the current polarity: $1A^+$, $1C^-$, $2C^-$, $2B^+$, $3B^+$, $3A^-$, $4A^-$, $4C^+$, $5C^+$, $5B^-$, $6B^-$, and $6A^+$, as shown in *figure 3(b)* To satisfy the OC, the switching-state patterns of active vectors in sectors where the corresponding phase current reaches its positive maximum (indicated by "+") remain identical to those in the conventional space vector diagram. In contrast, for sectors where the phase current reaches its negative maximum (indicated by "–"), the switching logic of the active vectors must be inverted, as represented by the red markings in the yellow regions. From the redesigned switching-state configuration based on the space vector diagram for controlling the CPSs in each bridge arm of the proposed Vienna T-type rectifier, as shown in *figure 3(b)*, it can be observed that the synthesis of the rotating reference voltage vector across the twelve updated sectors (k) involves four associated vectors per sector—two active and two zero vectors—hereafter referred to as the nearest four vectors. For example, in the first updated sector ($1A^+$), spanning 0°–30°, the nearest four vectors consist of $\vec{V}_0$, $\vec{V}_1$, $\vec{V}_2$, and $\vec{V}_7$, which satisfy the steady-state modulation condition.

Table 1. Symmetrically switching sequences based on the nearest four vectors

Sectors (k)	Nearest four vectors	Switching sequences	Sectors (k)	Nearest four vectors	Switching sequences
$1A^+$	$\vec{V}_0$, $\vec{V}_1$, $\vec{V}_2$, $\vec{V}_7$	000-100-110-111-110-100-000	$1C^-$	$\vec{V}_0$, $\vec{V}_1$, $\vec{V}_2$, $\vec{V}_7$	000-001-011-111-011-001-000
$2C^-$	$\vec{V}_0$, $\vec{V}_2$, $\vec{V}_3$, $\vec{V}_7$	000-001-101-111-101-001-000	$2B^+$	$\vec{V}_0$, $\vec{V}_2$, $\vec{V}_3$, $\vec{V}_7$	000-010-110-111-110-010-000
$3B^+$	$\vec{V}_0$, $\vec{V}_3$, $\vec{V}_4$, $\vec{V}_7$	000-010-011-111-011-010-000	$3A^-$	$\vec{V}_0$, $\vec{V}_3$, $\vec{V}_4$, $\vec{V}_7$	000-100-101-111-101-100-000
$4A^-$	$\vec{V}_0$, $\vec{V}_4$, $\vec{V}_5$, $\vec{V}_7$	000-100-110-111-110-100-000	$4C^+$	$\vec{V}_0$, $\vec{V}_4$, $\vec{V}_5$, $\vec{V}_7$	000-001-011-111-011-001-000
$5C^+$	$\vec{V}_0$, $\vec{V}_5$, $\vec{V}_6$, $\vec{V}_7$	000-001-101-111-101-001-000	$5B^-$	$\vec{V}_0$, $\vec{V}_5$, $\vec{V}_6$, $\vec{V}_7$	000-010-110-111-110-010-000
$6B^-$	$\vec{V}_0$, $\vec{V}_1$, $\vec{V}_6$, $\vec{V}_7$	000-010-011-111-011-010-000	$6A^+$	$\vec{V}_0$, $\vec{V}_1$, $\vec{V}_6$, $\vec{V}_7$	000-100-101-111-101-100-000

The vector sequence is set up so that the same vector starts and ends the sequence. This is to avoid having to switch between different carrier periods. Moreover, only one phase leg is allowed to change its switching state at a time to minimize switching losses and simplify commutation. Under these constraints, the optimal low-CMV sequence derived from the nearest four vectors is 000–100–110–111–110–100–000, forming a seven-segment symmetrical pattern centered around the reference vector and beginning and ending with the zero vector (000). *Table 1* presents a complete summary of the seven-segment symmetrical switching sequences generated from the nearest four vectors across all twelve updated sectors. This configuration ensures continuous modulation, a balanced NP voltage, and reduced CMV, while maintaining a simple structure and high computational efficiency suitable for digital implementation.

4.2. Design of Simplified Continuous PWM Generation with Zero-Sequence Signal Injection

According to the nearest four-vector synthesis principle, each conventional sector comprises two active and two zero vectors located closest to the $\vec{V}_{ref}$. The average value of $\vec{V}_{ref}$ is synthesized based on the volt-second balance principle of the SVM strategy. For instance, when $\vec{V}_{ref}$ lies within the first conventional sector (0°–60°), the effective $\vec{V}_{ref}$ can be expressed as

$$\vec{V}_{ref}T_S = \vec{V}_1 t_1 + \vec{V}_2 t_2 \tag{4}$$

where t_1 and t_2 denote the dwell times of the active vectors $\vec{V}_1$ and $\vec{V}_2$, respectively. The vector projection along the α- and β-axes yields

$$\vec{V}_{ref}T_S = \left(\sqrt{\frac{2}{3}}v_\alpha\right)t_1 + \left(\frac{1}{\sqrt{6}}v_\alpha + \frac{1}{\sqrt{2}}v_\beta\right)t_2 \tag{5}$$

Decomposing (5) into its α- and β-components gives the dwell times as

$$t_1 = \sqrt{\frac{3}{2}}v_\alpha T_S - \frac{1}{\sqrt{2}}v_\beta T_S,\ t_2 = \sqrt{2}v_\beta T_S \tag{6}$$

The zero-vector dwell time, represented as $T_0 = t_0 + t_7$, is then calculated as follows:

$$T_0 = T_S - \sqrt{\frac{3}{2}}v_\alpha T_S - \frac{1}{\sqrt{2}}v_\beta T_S \tag{7}$$

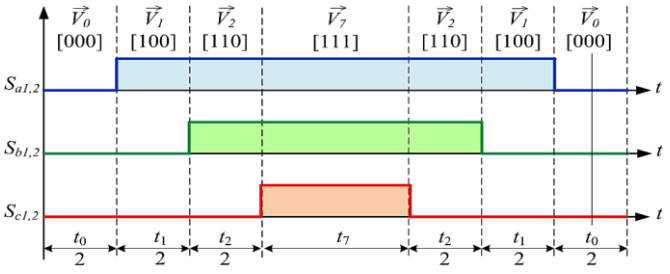

Figure 4. Symmetrically switch driving signal sequences for the first updated sector (0°-30°)

FOREX Publication
Open Access | Rapid and quality publishing
International Journal of Electrical and Electronics Research (IJEER)
Research Article | Volume 14, Issue 1| Pages 64-72|e-ISSN: 2347-470X

For the first updated sector ($1A^+$), the proposed symmetrical switching sequence is determined based on the nearest four vectors, and the corresponding switching signals are shown in *figure 4*. The conduction intervals for each of the bridge arms, T_a, T_b, and T_c, are defined as follows:

$$T_a = t_1 + t_2 + \frac{T_0}{2}, T_b = t_2 + \frac{T_0}{2}, T_c = \frac{T_0}{2} \quad (8)$$

Using the projections of the reference voltage vectors in the $\alpha\beta$-plane and calculating the modulation waveforms as the ratio between the total conduction duration of each CPS and the switching period, the continuous modulation waveform equations for the first updated sector are derived as

$$\begin{aligned} v_{ma} &= \frac{1}{2} + \frac{\sqrt{3}}{2\sqrt{2}} m_\alpha + \frac{1}{2\sqrt{2}} m_\beta, \\ v_{mb} &= \frac{1}{2} - \frac{\sqrt{3}}{2\sqrt{2}} m_\alpha + \frac{3}{2\sqrt{2}} m_\beta, \\ v_{mc} &= \frac{1}{2} - \frac{\sqrt{3}}{2\sqrt{2}} m_\alpha - \frac{1}{2\sqrt{2}} m_\beta \end{aligned} \quad (9)$$

In the $\alpha\beta$-plane, the modulating waves are defined as $m_\alpha = v_\alpha/v_{dc}$ and $m_\beta = v_\beta/v_{dc}$. The modulation waveforms for all updated sectors are derived by first analyzing the initial sector ($1A^+$) and then systematically rotating the reference voltage vector while reassigning the corresponding nearest four vectors according to *fig. 3(b)* and *table 1*. The resulting dwell times are mapped onto a symmetrical seven-segment switching sequence to determine the conduction intervals of the three-phase legs. For a given sector k, the continuous modulation signals are finally obtained by normalizing the total conduction duration of each phase leg with respect to the switching period:

$$v_{mx}^{(k)} = \frac{T_x^{(k)}}{T_S}, \quad x \in \{a, b, c\} \quad (10)$$

where $T_x^{(k)}$ is the total conduction duration of phase x in sector k. Substituting the dwell-time expressions and applying the vector projections in the $\alpha\beta$-plane, the phase modulation signals can be directly expressed as linear combinations of m_α and m_β. The resulting analytical expressions for all twelve updated sectors are summarized in *table 2*.

Table 2. The three-phase modulation signal equations for the twelve updated sectors

Sector (k)	Modulation Waveform Equations	Sector (k)	Modulation Waveform Equations
$1A^+$	$v_{ma} = \frac{1}{2} + \frac{\sqrt{3}}{2\sqrt{2}} m_\alpha + \frac{1}{2\sqrt{2}} m_\beta,$ $v_{mb} = \frac{1}{2} - \frac{\sqrt{3}}{2\sqrt{2}} m_\alpha + \frac{3}{2\sqrt{2}} m_\beta,$ $v_{mc} = \frac{1}{2} - \frac{\sqrt{3}}{2\sqrt{2}} m_\alpha - \frac{1}{2\sqrt{2}} m_\beta$	$4A^-$	$v_{ma} = \frac{1}{2} - \frac{\sqrt{3}}{2\sqrt{2}} m_\alpha - \frac{1}{2\sqrt{2}} m_\beta,$ $v_{mb} = \frac{1}{2} + \frac{\sqrt{3}}{2\sqrt{2}} m_\alpha - \frac{3}{2\sqrt{2}} m_\beta,$ $v_{mc} = \frac{1}{2} + \frac{\sqrt{3}}{2\sqrt{2}} m_\alpha + \frac{1}{2\sqrt{2}} m_\beta$
$1C^-$	$v_{ma} = \frac{1}{2} - \frac{\sqrt{3}}{2\sqrt{2}} m_\alpha - \frac{1}{2\sqrt{2}} m_\beta,$ $v_{mb} = \frac{1}{2} + \frac{\sqrt{3}}{2\sqrt{2}} m_\alpha - \frac{3}{2\sqrt{2}} m_\beta,$ $v_{mc} = \frac{1}{2} + \frac{\sqrt{3}}{2\sqrt{2}} m_\alpha + \frac{1}{2\sqrt{2}} m_\beta$	$4C^+$	$v_{ma} = \frac{1}{2} + \frac{\sqrt{3}}{2\sqrt{2}} m_\alpha + \frac{1}{2\sqrt{2}} m_\beta,$ $v_{mb} = \frac{1}{2} - \frac{\sqrt{3}}{2\sqrt{2}} m_\alpha + \frac{3}{2\sqrt{2}} m_\beta,$ $v_{mc} = \frac{1}{2} - \frac{\sqrt{3}}{2\sqrt{2}} m_\alpha - \frac{1}{2\sqrt{2}} m_\beta$
$2C^-$	$v_{ma} = \frac{1}{2} - \frac{\sqrt{3}}{\sqrt{2}} m_\alpha,$ $v_{mb} = \frac{1}{2} - \frac{1}{\sqrt{2}} m_\beta,$ $v_{mc} = \frac{1}{2} + \frac{1}{\sqrt{2}} m_\beta$	$5C^+$	$v_{ma} = \frac{1}{2} + \frac{\sqrt{3}}{\sqrt{2}} m_\alpha,$ $v_{mb} = \frac{1}{2} + \frac{1}{\sqrt{2}} m_\beta,$ $v_{mc} = \frac{1}{2} - \frac{1}{\sqrt{2}} m_\beta$
$2B^+$	$v_{ma} = \frac{1}{2} + \frac{\sqrt{3}}{\sqrt{2}} m_\alpha,$ $v_{mb} = \frac{1}{2} + \frac{1}{\sqrt{2}} m_\beta,$ $v_{mc} = \frac{1}{2} - \frac{1}{\sqrt{2}} m_\beta$	$5B^-$	$v_{ma} = \frac{1}{2} - \frac{\sqrt{3}}{\sqrt{2}} m_\alpha,$ $v_{mb} = \frac{1}{2} - \frac{1}{\sqrt{2}} m_\beta,$ $v_{mc} = \frac{1}{2} + \frac{1}{\sqrt{2}} m_\beta$

FOREX Publication
Open Access | Rapid and quality publishing
International Journal of Electrical and Electronics Research (IJEER)
Research Article | Volume 14, Issue 1| Pages 64-72|e-ISSN: 2347-470X

3B$^+$	$v_{ma}=\frac{1}{2}+\frac{\sqrt{3}}{2\sqrt{2}}m_\alpha-\frac{1}{2\sqrt{2}}m_\beta,$ $v_{mb}=\frac{1}{2}-\frac{\sqrt{3}}{2\sqrt{2}}m_\alpha+\frac{1}{2\sqrt{2}}m_\beta,$ $v_{mc}=\frac{1}{2}-\frac{\sqrt{3}}{2\sqrt{2}}m_\alpha-\frac{3}{2\sqrt{2}}m_\beta$	6B$^-$	$v_{ma}=\frac{1}{2}-\frac{\sqrt{3}}{2\sqrt{2}}m_\alpha+\frac{1}{2\sqrt{2}}m_\beta,$ $v_{mb}=\frac{1}{2}+\frac{\sqrt{3}}{2\sqrt{2}}m_\alpha-\frac{1}{2\sqrt{2}}m_\beta,$ $v_{mc}=\frac{1}{2}+\frac{\sqrt{3}}{2\sqrt{2}}m_\alpha+\frac{3}{2\sqrt{2}}m_\beta$
3A$^-$	$v_{ma}=\frac{1}{2}-\frac{\sqrt{3}}{2\sqrt{2}}m_\alpha+\frac{1}{2\sqrt{2}}m_\beta,$ $v_{mb}=\frac{1}{2}+\frac{\sqrt{3}}{2\sqrt{2}}m_\alpha-\frac{1}{2\sqrt{2}}m_\beta,$ $v_{mc}=\frac{1}{2}+\frac{\sqrt{3}}{2\sqrt{2}}m_\alpha+\frac{3}{2\sqrt{2}}m_\beta$	6A$^+$	$v_{ma}=\frac{1}{2}+\frac{\sqrt{3}}{2\sqrt{2}}m_\alpha-\frac{1}{2\sqrt{2}}m_\beta,$ $v_{mb}=\frac{1}{2}-\frac{\sqrt{3}}{2\sqrt{2}}m_\alpha+\frac{1}{2\sqrt{2}}m_\beta,$ $v_{mc}=\frac{1}{2}-\frac{\sqrt{3}}{2\sqrt{2}}m_\alpha-\frac{3}{2\sqrt{2}}m_\beta$

It should be noted that *table 2* is obtained through cyclic permutation of phase variables and sign inversion of the modulation components, depending on the polarity of the dominant phase current. For sectors labeled with "+," the modulation equations follow the conventional SVM orientation, whereas for sectors labeled with "–," the corresponding expressions are derived by inverting the active vector sequence to satisfy the OC. Consequently, all twelve modulation equations share a unified mathematical structure, differing only by phase rotation and sign assignment. However, the three-phase modulation signals derived from *table 2* cannot be directly applied to satisfy the OC of the Vienna T-type rectifier, as the original command signals do not fully comply with the rectifier's OR. Hence, a zero-sequence component (v_0) is injected into each phase modulation signal, producing modified modulation wave equations expressed as

$$v'_{ma}=v_{ma}+v_0, v'_{mb}=v_{mb}+v_0, v'_{mc}=v_{mc}+v_0 \quad (11)$$

The injected zero-sequence component is obtained by analyzing the deviation between the original modulation signals and the OC condition. According to the OC, the CPSs in the bridge arm corresponding to the phase with the highest instantaneous input current—during both positive and negative half-cycles—must remain in clamping mode. Consequently, the modulation signals are offset upward such that their peak values are clamped at logic "1" throughout the conduction interval. The amplitude of the modulation signals is further scaled in proportion to the modulation index of the SVM. Therefore, the definition of the zero-sequence component is as follows:

$$v_0=\frac{1}{2}-\frac{m_a}{2} \quad (12)$$

where m_a is the SVM modulation index ($0<m_a\leq 1$), calculated from the reference voltage and DC-link voltage as

$$m_a=\frac{\sqrt{3}V_{ref}}{V_{dc}} \quad (13)$$

The zero-sequence component defined in *equation (12)* is uniformly applied across all twelve updated sectors to ensure proper switching-state alignment with the OC. The resulting modified modulation signals enable accurate continuous PWM generation, maintain NP voltage balance, and significantly reduce CMV. Finally, the gate signals for the CPSs are generated by comparing the modified modulation waveforms with a triangular carrier using a standard PWM comparator.

Table 3. Main parameters of the Vienna T-type rectifier

Parameters	Symbols	Value
AC input voltage (RMS)	e_a, e_b, and e_c	110 V
DC-Link voltage	V_{dc}	600 V
Line frequency	f_L	50 Hz
Switching frequency	f_s	12 kHz
Input inductance	L_a, L_b, and L_c	5 mH
Input resistance	R_a, R_b, and R_c	5 Ω
Rated power	P_{Rated}	5 kW
DC-link capacitance	C_1, and C_2	2200 μF

5. RESULTS AND DISCUSSION

The performance of the proposed simplified continuous PWM strategy, developed using the nearest four vectors derived from the 2L-SVM principle, was evaluated through detailed simulations conducted in MATLAB/Simulink. For benchmarking, the conventional discontinuous SVPWM method based on the 12-sector equivalent SVM configuration was implemented under identical operating conditions. Both methods were assessed in terms of input current quality, DC-link voltage regulation, and CMV characteristics. The simulation model of the Vienna T-type rectifier was configured using the parameters listed in *table 3*.

FOREX Publication
Open Access | Rapid and quality publishing
International Journal of Electrical and Electronics Research (IJEER)
Research Article | Volume 14, Issue 1| Pages 64-72|e-ISSN: 2347-470X

Figure 5 shows the steady-state input characteristics of the conventional discontinuous SVPWM and the proposed continuous PWM strategies. For the conventional discontinuous SVPWM in *figure 5(a)–(d)*, the pole voltage (v_{aO}) and line-to-line voltage (v_{ab}) exhibit three discrete levels corresponding to half of the DC-link voltage. The discontinuous operation, characterized by the zero clamping of one phase leg during intervals when its input current reaches the highest instantaneous value, inherently satisfies the OC of the Vienna T-type rectifier. As a result, the three-phase input currents are symmetrical and almost sinusoidal, with a THD of 2.16% and a fundamental amplitude of 22.63 A. In contrast, the proposed continuous PWM strategy in *figure 5(e)–(h),* maintains a continuous modulation pattern in the pole voltage (v_{aO}) while preserving the same three voltage levels of $\pm V_{dc}/2$ and 0. The corresponding line-to-line voltage (v_{ab}) shows a smoother five-level waveform, which improves voltage resolution, reduces high-frequency components, and enhances overall power quality. Although slight waveform distortions appear near the intervals of maximum instantaneous current—attributed to the absence of strict phase clamping under continuous operation—the resulting input current THD of 2.49% remains well within the IEEE 519 limit (< 5%). This confirms that the proposed method achieves comparable current quality while offering superior voltage waveform smoothness compared with the conventional approach.

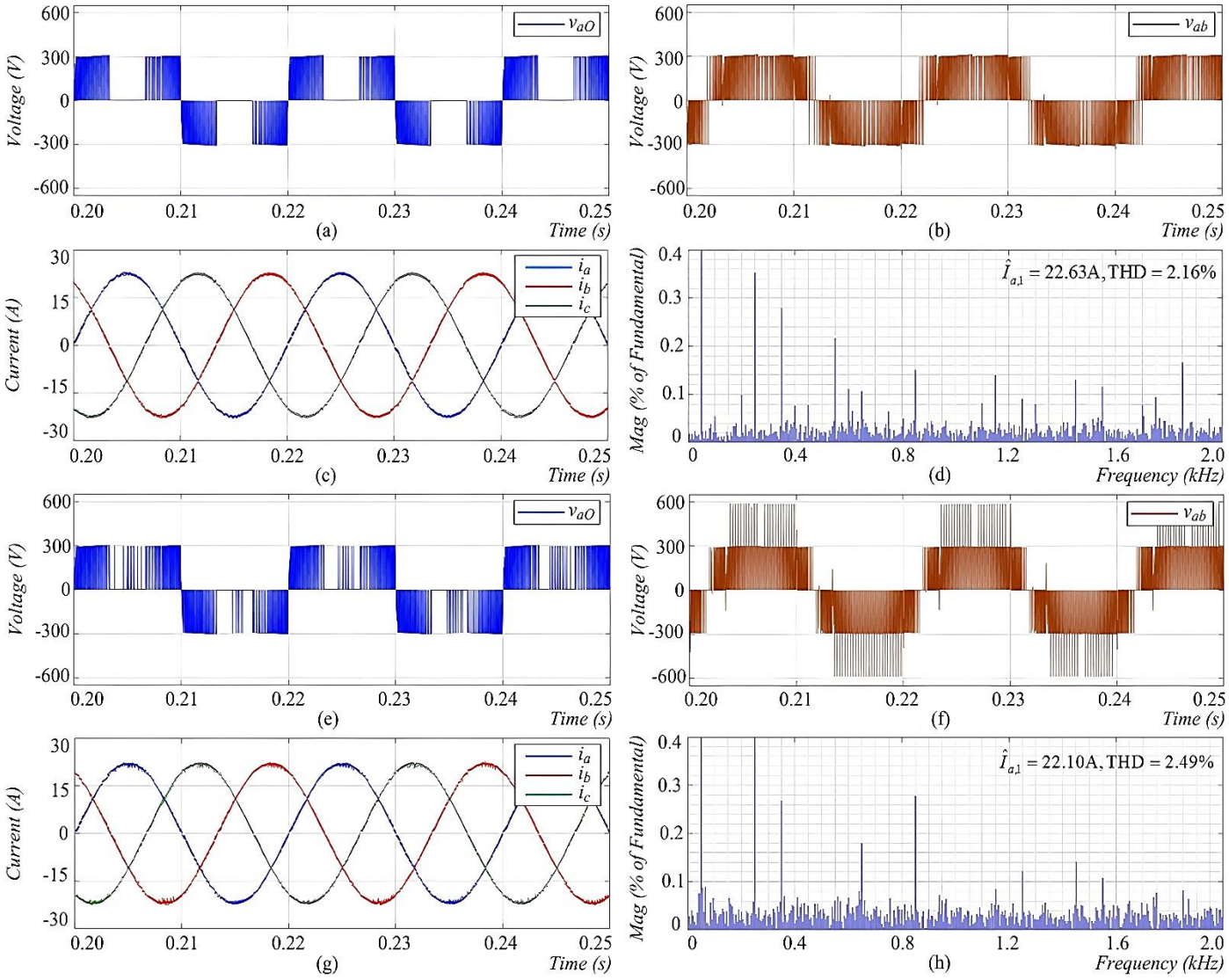

Figure 5. Comparison of steady-state input characteristics between the conventional method and the proposed method: *(a)-(d)* Conventional discontinuous SVPWM method, *(e)-(h)* Proposed method

FOREX Publication
Open Access | Rapid and quality publishing
International Journal of Electrical and Electronics Research (IJEER)
Research Article | Volume 14, Issue 1| Pages 64-72|e-ISSN: 2347-470X

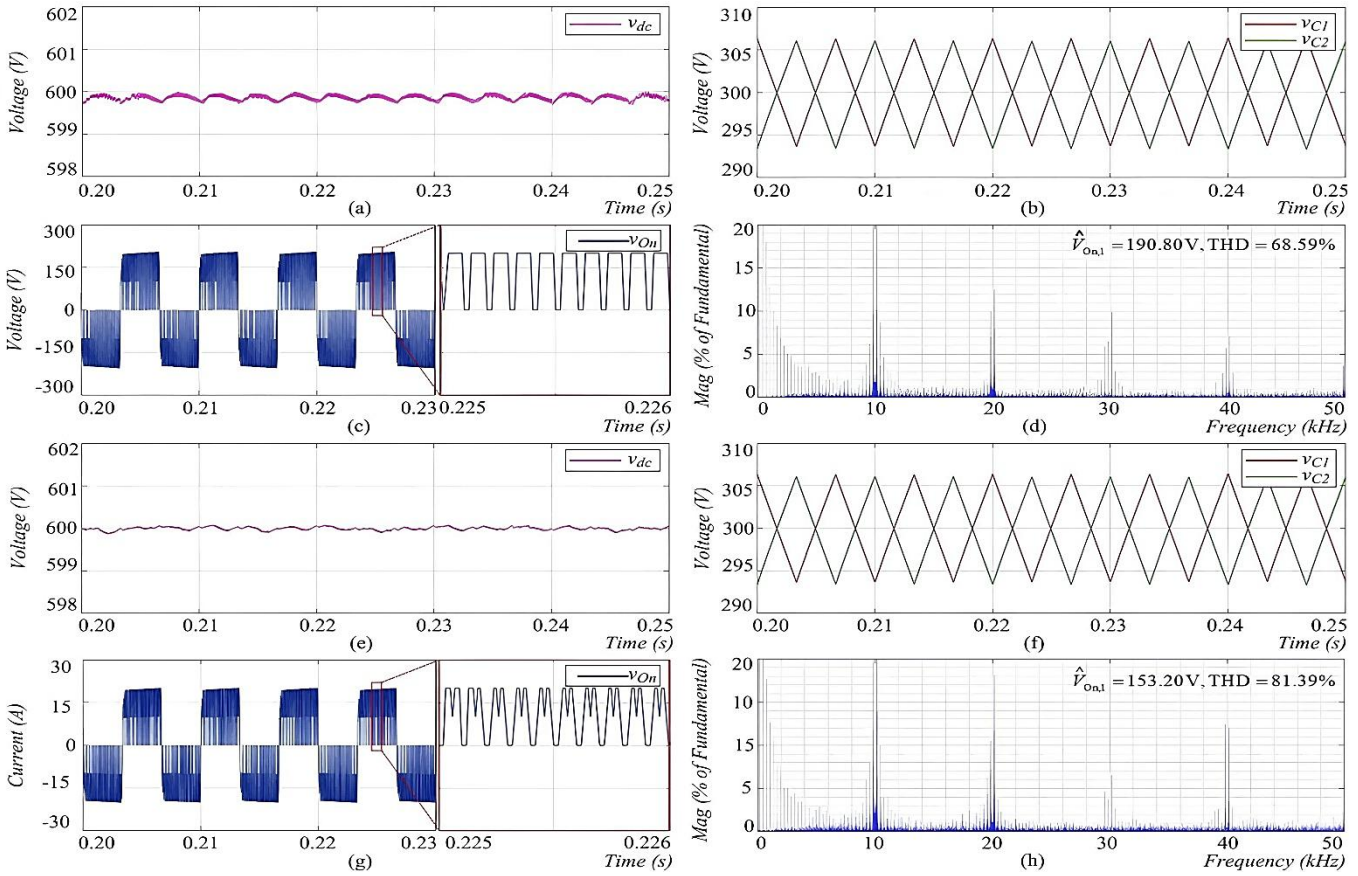

Figure 6. Comparison of steady-state output characteristics between the conventional method and the proposed method: (a)-(d) Conventional discontinuous SVPWM method, (e)-(h) Proposed method

Figure 6 compares the steady-state output characteristics of both modulation strategies. For the conventional discontinuous SVPWM in *figure 6(a)–(d)*, the DC-link voltage (v_{dc}) remains nearly constant at 600 V. The voltages across the split DC-link capacitors (v_{C1} and v_{C2}) maintain symmetry at half of the DC-link voltage, indicating effective NP voltage balance. The corresponding CMV has a five-level waveform: ±Vdc/3, ±Vdc/6, and 0. It oscillates at three times the line frequency and has a fundamental amplitude of 190.80 V and an RMS value of 134.91 V, which is in line with the analytical results in *section 3*. In contrast, the proposed continuous PWM method in *figure 6(e)–(h)*, employs symmetrical seven-segment switching sequences derived from the nearest four vectors. The DC-link voltage (v_{dc}) is also regulated at 600 V, and the split capacitor voltages remain well balanced, confirming stable NP potential and improved voltage symmetry. The CMV retains its five-level pattern with a triple frequency component; however, as shown in the magnified view of *figure 6(g)*, the CMV magnitude at the center of each half-cycle exhibits two distinct amplitude levels, $+V_{dc}/6$ and $+V_{dc}/3$, throughout the switching period—unlike the conventional discontinuous SVPWM, which maintains a higher single amplitude of $+V_{dc}/3$. Consequently, the proposed strategy achieves a 19.71% reduction in the level of CMV value compared with the conventional method. This improvement results from the smoother voltage transitions achieved through the continuous PWM technique incorporating a symmetric seven-segment sequence and zero-sequence voltage injection. These features effectively suppress abrupt switching transitions and CMV spikes, leading to lower dv/dt stress, reduced leakage current, and mitigated EMI. Such characteristics make the proposed strategy particularly suitable for grid-connected converters and EV fast-charging systems, where enhanced electromagnetic compatibility (EMC), high reliability, and superior power quality are critical performance criteria.

In practical digital implementation, the proposed modulation strategy can be readily realized using standard DSP or FPGA platforms, as it relies only on algebraic computation of modulation signals and a conventional CB-PWM comparator. Unlike optimization-based nearest four-vector approaches, the proposed method does not require iterative duty-cycle adjustment or sector-dependent switching sequence reconstruction, thereby reducing computational burden and enabling real-time execution at typical switching frequencies used in Vienna rectifiers. During experimental operation, the symmetrical seven-segment switching sequence is expected to produce smoother pole and line-to-line voltage waveforms, consistent with the simulation results. Moreover, since the proposed approach preserves the conventional VOC structure, no modification of the outer control loops is required. Only the PWM generation stage is replaced, which facilitates straightforward integration into existing Vienna T-Type rectifier control platforms. Minor deviations between simulation and experimental results may arise from device non-idealities and measurement noise; however, the overall CMV reduction trend and power-quality improvement are expected to remain consistent.

FOREX Publication
Open Access | Rapid and quality publishing
International Journal of Electrical and Electronics Research (IJEER)
Research Article | Volume 14, Issue 1| Pages 64-72|e-ISSN: 2347-470X

CONCLUSION

This paper has presented a simplified continuous PWM strategy for the Vienna T-type rectifier, constructed from the nearest four vectors of the 2L-SVM diagram and enhanced through a unified zero-sequence injection approach. The redesigned twelve-sector switching-state configuration ensures compliance with the operating constraint (OC), enables continuous voltage modulation, and inherently maintains neutral-point (NP) voltage balance without auxiliary control. Simulation results verified that the proposed method provides clear advantages over the conventional discontinuous SVPWM. It makes five-level line-to-line voltage waveforms smoother, lowers CMV RMS amplitude by 19.71%, and keeps the input current quality high while keeping THD within IEEE 519 limits. In addition, the simplified analytical formulation and carrier-based implementation facilitate real-time realization on standard digital platforms. Moreover, owing to the continuous PWM structure and unified zero-sequence regulation, the proposed strategy exhibits strong robustness under practical non-ideal operating conditions. The symmetrical switching sequence preserves DC-link voltage balance and limits CMV-induced dv/dt stress, thereby enhancing tolerance to EMI and leakage currents. Consequently, stable operation and consistent CMV reduction performance are expected in realistic grid-connected environments. Overall, these results indicate that the proposed continuous PWM approach provides an effective, robust, and implementation-friendly solution for high-efficiency applications such as EV fast charging, renewable energy interfaces, and grid-connected power conversion systems.

REFERENCES

[1] Zheng, K.; Hou, Y.; Wang, X.; Liu, Y. An active rectifier with pulse width modulation (PWM) mode on-and off-delay compensation for wireless power transfer (WPT) system. IEEE Access 2023, 11, 118204-118216.

[2] Zhang, D.; Leontaris, C.; Huber, J.; Kolar, J. W. Optimal synergetic control of three-phase/level boost–buck voltage DC-link AC/DC converter for very-wide output voltage range high-efficiency EV charger. IEEE Journal of Emerging and Selected Topics in Power Electronics 2023, 12(1), 28-42.

[3] Zhou, N.; Wang, J.; Wang, Q.; Wei, N. Measurement-based harmonic modeling of an electric vehicle charging station using a three-phase uncontrolled rectifier. IEEE Transactions on Smart Grid 2014, 6(3), 1332-1340.

[4] Soeiro, T. B.; Kolar, J. W. Analysis of high-efficiency three-phase two- and three-level unidirectional hybrid rectifiers. IEEE Transactions on Industrial Electronics 2012, 60(9), 3589-3601.

[5] Hariprasad, B.; Sreenivasan, G.; Kumar, S. A.; Mallikarjuna, B. Vehicle-to-Grid Power Transfer Method for Electric Vehicles using off-board charger. IJEER 2024, 12(4), 1203-1210.

[6] Bharaneedharan, B.; Suresh, P.; Elumalai, P. V. Energy-efficient Vienna rectifier for electric vehicle battery charging stations. Results in Engineering 2024, 23, 102671.

[7] Zhang, P.; Wu, X.; Li, B., Ding, L.; Long, J.; Zhang, W.; Li, Y. Reduction of common-mode voltage and np voltage oscillation for three-level vienna rectifiers using alternative phase opposition disposition pwm. IEEE transactions on industrial electronics 2023, 71(8), 8237-8247.

[8] Foureaux, N. C.; Oliveira, J. H.; de Oliveira, F. D.; Cardoso Filho, B. D. J.; de Faria, R. S. Command generation for wide-range operation of hysteresis-controlled Vienna rectifiers. IEEE Transactions on Industry Applications 2014, 51(3), 2373-2380.

[9] Lee, J. S.; & Lee, K. B. A novel carrier-based PWM method for Vienna rectifier with a variable power factor. IEEE Trans. Ind. Electron 2016, 63(1), 3-12.

[10] Hang, L.; Li, B.; Zhang, M.; Wang, Y.; Tolbert, L. M. Equivalence of SVM and carrier-based PWM in three-phase/wire/level Vienna rectifier and capability of unbalanced-load control. IEEE Transactions on Industrial Electronics 2013, 61(1), 20-28.

[11] Ma, H.; Lu, Y.; Zheng, K.; Xu, T. Research on the simplified SVPWM for three-phase/switches Y-type two-level rectifier. IEEE Access 2020, 8, 214310-214321.

[12] Tubburee, O.; Photong, C.; Angkawisittpan, N.; Ek-iam, K.; Sangiamvibool, W. Design and Development of Three-Phase Two-Level Unidirectional Rectifiers for EV Chargers Using SVPWM and a Voltage-Oriented Controller. Engineering, Technology & Applied Science Research 2025, 15(5), 27877-27884.

[13] Xing, X.; Li, X.; Qin, C.; Liu, Z.; Zhang, C. Two-layer pulsewidth modulation strategy for common-mode voltage and current harmonic distortion reduction in Vienna rectifier. IEEE Transactions on Industrial Electronics 2019, 67(9), 7470-7483.

[14] Morris, C. T.; Han, D.; Sarlioglu, B. Reduction of common mode voltage and conducted EMI through three-phase inverter topology. IEEE Trans. Power Electron 2017, 32(3), 1720-1724.

[15] Zhang, Z.; Ding, D.; Li, B., Wang, G.; Shao, H.; Shi, B.; Xu, D. Common-mode voltage reduction modulation strategy based on nearest four voltage vectors optimization for vienna rectifier. IEEE transactions on power electronics 2023, 39(3), 2954-2965.

[16] Al-Ogaili, A. S.; Aris, I. B.; Verayiah, R.; Ramasamy, A.; Marsadek, M.; Rahmat, N. A.; Hoon, Y.; Aljanad, A.; Al-Masri, A. N. A three-level universal electric vehicle charger based on voltage-oriented control and pulse-width modulation. Energies 2019, 12(12), 1-20.